applied sciences

MDPI

Article

Transverse Spin Hall Effect and Twisted Polarization Ribbons at the Sharp Focus

Victor V. Kotlyar [1,2], Alexey A. Kovalev [1,2,*], Alexey M. Telegin [2], Elena S. Kozlova [1,2], Sergey S. Stafeev [1,2], Alexander Kireev [3], Kai Guo [3] and Zhongyi Guo [3]

1 Image Processing Systems Institute, NRC "Kurchatov Institute", 151 Molodogvardeyskaya Str., Samara 443001, Russia; kotlyar@ipsiras.ru (V.V.K.); kozlova.elena.s@gmail.com (E.S.K.); stafeev@ipsiras.ru (S.S.S.)
2 Technical Cybernetics Department, Samara National Research University, 34 Moskovskoye Shosse, Samara 443086, Russia; talex85@mail.ru
3 School of Computer Science and Information Engineering, Hefei University of Technology, No. 485, Danxia Road, Shushan District, Hefei 230009, China; al3xanders1lver@gmail.com (A.K.); guozhongyi@hfut.edu.cn (Z.G.)
* Correspondence: alanko@ipsiras.ru

Abstract: In this work, using a Richards-Wolf formalism, we derive explicit analytical relationships to describe vectors of the major and minor axes of polarization ellipses centered in the focal plane when focusing a cylindrical vector beam of integer order n. In these beams, the major axis of a polarization ellipse is found to lie in the focal plane, with the minor axis being perpendicular to the focal plane. This means that the polarization ellipse is perpendicular to the focal plane, with its polarization vector rotating either clockwise or anticlockwise and forming "photonic wheels". Considering that the wave vector is also perpendicular to the focal plane, we conclude that the polarization ellipse and the wave vector are in the same plane, so that at some point these can coincide, which is uncharacteristic of transverse electromagnetic oscillations. In a cylindrical vector beam, the spin angular momentum vector lies in the focal plane, so when making a circle centered on the optical axis, at some sections, the handedness of the spin vector and circular motion are the same, being opposite elsewhere. This effect may be called an azimuthal transverse spin Hall effect, unlike the familiar longitudinal spin Hall effect found at the sharp focus. The longitudinal spin Hall effect occurs when opposite-sign longitudinal projections of the spin angular momentum vector are spatially separated in the focal plane. In this work, we show that for the latter, there are always an even number of spatially separated regions and that, when making an axis-centered circle, the major-axis vector of polarization ellipse forms a two-sided twisted surface with an even number of twists.

Keywords: Richards-Wolf formalism; sharp focus; polarization ellipses; cylindrical vector beam; spin angular momentum; photonic wheels; transverse spin Hall effect; polarization stripe; twisted surface

Citation: Kotlyar, V.V.; Kovalev, A.A.; Telegin, A.M.; Kozlova, E.S.; Stafeev, S.S.; Kireev, A.; Guo, K.; Guo, Z. Transverse Spin Hall Effect and Twisted Polarization Ribbons at the Sharp Focus. *Appl. Sci.* **2024**, *14*, 3926. https://doi.org/10.3390/app14093926

Academic Editor: Luca Poletto

Received: 19 March 2024
Revised: 27 April 2024
Accepted: 30 April 2024
Published: 4 May 2024

1. Introduction

Previously, an experimental observation of a polarization Mobius ribbon at the sharp focus of a vector laser beam generated with a q-plate has been reported [1]. The polarization Mobius ribbon was shown to make 3 half-twists at the tight focus of an initial optical vortex with topological charge $n = 1$, making 5 half-twists at $n = 3$. A technique for generating exotic polarization Mobius ribbons has been numerically demonstrated [2], and the generation of polarization Mobius ribbons upon focusing tilted vector beams has been studied [3]. Alongside one-sided polarization Mobius ribbons, it has been found that paraxial and non-paraxial vector beams can also form two-sided twist bands with an even number of twists [4–7].

On the other hand, as far as the spin Hall effect at the focus is concerned [8–10], it has been shown that with increasing topological charge of vector vortex beams, the number of focal regions with alternating spin signs also increases. Such opposite-sign focal regions occur in pairs, so the general spin of the beams remains zero, meaning that the number of opposite-sign regions lying on an axis-centered circle is always even. Therefore, by making a full circle in the focal plane, the polarization ellipse makes an even number of semi-turns, i.e., an integer number of full turns. Meanwhile, a surface generated by the major/minor-axis vector of the polarization ellipse is not a one-sided Mobius ribbon, as was the case in Refs. [1,2], but a two-sided surface with an even number of semi-turns [4]. Such polarization ribbons have been given the name twisted ribbons [4].

The arrangement of polarization ellipses in the focal plane can be derived from an equation for the coordinates of the major and minor axes of the polarization ellipse proposed by M. Berry [11]. As a rule, the major and minor axes of polarization ellipses are calculated numerically. In the meantime, in this work we discuss two examples of vector fields (a cylindrical *n-th* order vector field and an azimuthally polarized optical vortex with topological charge n), for which we derive exact analytical relationships that describe coordinate distributions of the major and minor axes of polarization ellipses in the tight focus plane, based on a Richards-Wolf formalism [12].

2. Projections of Strength, Intensity and Spin Angular Momentum at the Tight Focus of a Light Field

Assume an original light field whose Jones vector is given by

$$\mathbf{E}(\varphi) = \exp(in\varphi)\begin{pmatrix} 1 \\ 0 \end{pmatrix}, \tag{1}$$

where (r, φ) are the polar coordinates at the beam cross-section, n is the integer topological charge, with the linear polarization vector being directed along the horizontal x-axis. Projections of the electric and magnetic field vectors at the focus of the original field in Equation (1) are given by [13]

$$\begin{aligned} E_x &= \tfrac{i^{n-1}}{2} e^{in\varphi} \left(2I_{0,n} + e^{2i\varphi} I_{2,n+2} + e^{-2i\varphi} I_{2,n-2}\right), \\ E_y &= \tfrac{i^n}{2} e^{in\varphi} \left(e^{-2i\varphi} I_{2,n-2} - e^{2i\varphi} I_{2,n+2}\right), \\ E_z &= i^n e^{in\varphi} \left(e^{-i\varphi} I_{1,n-1} - e^{i\varphi} I_{1,n+1}\right), \end{aligned} \tag{2}$$

Entering Equation (2) are the functions $I_{\mu\nu}$ of a single radial variable r:

$$I_{\nu,\mu} = 2kf \int_0^\alpha \sin^{\nu+1}\left(\frac{\theta}{2}\right) \cos^{3-\nu}\left(\frac{\theta}{2}\right) \cos^{1/2}(\theta) A(\theta) e^{ikz\cos\theta} J_\mu(kr\sin\theta) d\theta, \tag{3}$$

where $k = 2\pi/\lambda$ is the wave number of monochromatic light of wavelength λ, f is the focal length of a focusing lens, α is the maximum angle of the incident ray with the optical axis, which defines the numerical aperture of an aplanatic lens, NA = sin α, $J_\nu(\xi)$ is the Bessel function of the first kind and ν-th order. $A(\theta)$ is a real function that defines the radially symmetric amplitude of the original field, which depends on the incidence angle θ of an outgoing ray from the original wavefront converging at the center of the focal plane.

Next, using Equation (2), we can derive all three projections of the SAM vector [14]:

$$\mathbf{S} = \frac{1}{8\pi\omega} \mathrm{Im}(\mathbf{E}^* \times \mathbf{E}), \tag{4}$$

where ω is the angular frequency of light. Hereafter, the constant $1/(8\pi\omega)$ is dropped.

Substituting (2) into (4) yields relationships for projections of the spin density vector or the spin angular momentum vector at the tight focus for the original field (1):

$$\begin{aligned}
&S_x = M(r)\sin\varphi + N(r)\sin 3\varphi,\\
&S_y = O(r)\cos\varphi + M(r)\cos\varphi + N(r)\cos 3\varphi,\\
&S_z = \tfrac{1}{2}(I_{2,n-2} - I_{2,n+2})(I_{2,n-2} + I_{2,n+2} + 2I_{0,n}\cos 2\varphi),\\
&M(r) = I_{1,n-1}I_{2,n-2} - I_{1,n+1}I_{2,n+2},\\
&N(r) = I_{1,n-1}I_{2,n+2} - I_{1,n+1}I_{2,n-2},\\
&O(r) = 2I_{0,n}(I_{1,n-1} - I_{1,n+1}).
\end{aligned} \tag{5}$$

By analogy, we can express the full intensity, $I = I_x + I_y + I_z = |E_x|^2 + |E_y|^2 + |E_z|^2$ and its separate components at the focus:

$$\begin{aligned}
&I_x = I_{0,n}^2 + \tfrac{1}{4}I_{2,n-2}^2 + \tfrac{1}{4}I_{2,n+2}^2 + \cos 2\varphi(I_{0,n}I_{2,n-2} + I_{0,n}I_{2,n+2}) + \tfrac{1}{4}I_{2,n-2}I_{2,n+2}\cos 4\varphi,\\
&I_y = \tfrac{1}{4}I_{2,n-2}^2 + \tfrac{1}{4}I_{2,n+2}^2 - \tfrac{1}{4}I_{2,n-2}I_{2,n+2}\cos 4\varphi,\\
&I_z = I_{1,n-1}^2 + I_{1,n+1}^2 - 2I_{1,n-1}I_{1,n+1}\cos 2\varphi,\\
&I = I_{0,n}^2 + \tfrac{1}{2}I_{2,n-2}^2 + \tfrac{1}{2}I_{2,n+2}^2 + I_{1,n-1}^2 + I_{1,n+1}^2 + \cos 2\varphi(I_{0,n}I_{2,n-2} + I_{0,n}I_{2,n+2} - 2I_{1,n-1}I_{1,n+1}).
\end{aligned} \tag{6}$$

3. Expressing the Field Strength Vector via Vectors of the Axes of the Polarization Ellipse

Formulae for calculating the polarization singularity indices of vector fields have previously been reported [11]. Using those formulae, the **E**-field vector can be expressed via vectors **A** and **B**, which are oriented along the major and minor axes of a polarization ellipse centered on a given space point:

$$\begin{aligned}
&\mathbf{E} = e^{i\gamma}(\mathbf{A} + i\mathbf{B}),\quad I = |\mathbf{A}|^2 + |\mathbf{B}|^2,\\
&\mathbf{A}\bullet\mathbf{B} = 0,\quad |\mathbf{A}| \geq |\mathbf{B}|,\\
&\gamma = \tfrac{1}{2}\arg(\mathbf{E}\bullet\mathbf{E}),\\
&\mathbf{A} = \tfrac{1}{\left|\sqrt{\mathbf{E}\bullet\mathbf{E}}\right|}\mathrm{Re}\left(\mathbf{E}\sqrt{\mathbf{E}^*\bullet\mathbf{E}^*}\right),\\
&\mathbf{B} = \tfrac{1}{\left|\sqrt{\mathbf{E}\bullet\mathbf{E}}\right|}\mathrm{Im}\left(\mathbf{E}\sqrt{\mathbf{E}^*\bullet\mathbf{E}^*}\right),\\
&\mathbf{S} = \mathrm{Im}(\mathbf{E}^* \times \mathbf{E}) = 2(\mathbf{A} \times \mathbf{B}).
\end{aligned} \tag{7}$$

In Equation (7), '•' denotes the dot product of vectors, $\times$ denotes the cross product, Re and Im are real and imaginary parts of the number, **S** simultaneously describes the SAM vector and the normal vector to the polarization ellipse plane formed by the vectors **A** and **B**, I is the intensity expressed through projections of the vectors of the polarization ellipse axes.

We note that the decomposition of the complex field **E** into the real vectors **A** and **B** is unambiguous, meaning that while not for any decomposition, the vectors **A** and **B** are mutually orthogonal, but for any decomposition, they lie in a perpendicular plane to the SAM vector, which is the polarization ellipse plane. Remarkably, representation (7) is also applicable to the light field at the focus defined by Equation (2), making it possible to derive explicit relationships for the two vectors **A** and **B** at the tight focus of field (1). Actually, the

E-field vector in (2) can be represented in a similar way to (7) by merely separating the real and imaginary parts:

$$\begin{aligned}
&\mathbf{E} = e^{i\gamma}(\mathbf{A} + i\mathbf{B}), \\
&A_x = I_{0,n} + P(r)\cos 2\varphi, \\
&A_y = P(r)\sin 2\varphi, \\
&A_z = F(r)\sin\varphi, \\
&B_x = Q(r)\sin 2\varphi, \\
&B_y = -Q(r)\cos 2\varphi, \\
&B_z = L(r)\cos\varphi, \\
&P(r) = (I_{2,n-2} + I_{2,n+2})/2, \;\; F(r) = I_{1,n-1} + I_{1,n+1}, \\
&Q(r) = (I_{2,n+2} - I_{2,n-2})/2, \;\; L(r) = I_{1,n-1} - I_{1,n+1}, \\
&\gamma = n\left(\varphi + \tfrac{\pi}{4}\right) - \tfrac{\pi}{4}.
\end{aligned} \tag{8}$$

Of course, the vectors **A** and **B** in (8) cannot be guaranteed to form two axes of the polarization ellipse at point (x, y, z = 0); however, it can be checked whether the derived projections of vectors in (8) enable obtaining the SAM projections in (5) and (6), because

$$\begin{aligned}
&\mathbf{S} = \mathrm{Im}(\mathbf{E}^* \times \mathbf{E}) = 2(\mathbf{A} \times \mathbf{B}), \\
&I = |\mathbf{A}|^2 + |\mathbf{B}|^2.
\end{aligned} \tag{9}$$

The SAM vector in (9) is perpendicular to the vectors **A** and **B**, with its absolute value being equal to the product of the modules of **A** and **B**, multiplied by the sine of an unknown angle η between the vectors:

$$|\mathbf{S}| = |\mathbf{A}||\mathbf{B}|\sin\eta. \tag{10}$$

From (10) it follows that linear polarization of field (1) at the focus corresponds to the zero modulus of either vector **A** or vector **B**: $|\mathbf{S}| = |\mathbf{A}| = |\mathbf{B}| = 0$. Equation (8) suggests that for any topological charge n, there exists an axis-centered radius r_0 of a circle in the focal plane (z = 0), such that the following equality holds:

$$2Q(r_0) = I_{2,n+2} - I_{2,n-2} = 0. \tag{11}$$

Along this circle in the focal plane, the vector **B** of the polarization ellipse has only a longitudinal projection:

$$\begin{aligned}
&B_x = Q(r_0)\sin 2\varphi = 0, \\
&B_y = -Q(r_0)\cos 2\varphi = 0, \\
&B_z = L(r_0)\cos\varphi.
\end{aligned} \tag{12}$$

Considering that the SAM vector in (9) is perpendicular to the vector **B**, the longitudinal projection of the SAM vector equals zero, and the SAM vector **S** lies in the focal plane. The vector **B** is of zero length at two points of a circle of radius r_0, namely, at $\varphi = \pi/2$ and $\varphi = 3\pi/2$, where $B_z = 0$. Let us analyze in more detail how the SAM vector varies in the neighborhood of those points. For instance, at angles slightly smaller than $\varphi = \pi/2$, the longitudinal projection of the **B** vector in (12) is positive ($L(r_0)\cos\varphi > 0$) at $L(r_0) > 0$, whereas at angles slightly larger than $\varphi = \pi/2$, the longitudinal projection of the vector **B** in (12) is negative ($L(r_0)\cos\varphi < 0$). The **A** vector is not found in the focal plane at points lying on the circle of radius r_0 and hardly changes its direction at angles smaller and larger than $\varphi = \pi/2$, being predominantly directed along the x-axis, as

$$\begin{aligned}
&A_x = I_{0,n}(r_0) + P(r_0)\cos 2\varphi \approx I_{0,n}(r_0) > 0, \\
&A_y = P(r_0)\sin 2\varphi \approx 0, \\
&A_z = F(r_0)\sin\varphi \approx F(r_0), \\
&I_{0,n}(r_0) >> P(r_0), I_{0,n}(r_0) >> F(r_0).
\end{aligned} \tag{13}$$

The inequalities in (13) are based on the results reported in Ref. [8]. Then, varying along the circle of radius r_0, the SAM vector will be near opposite to the vertical y-axis at angles slightly smaller than $\varphi = \pi/2$, being almost coincident with the vertical y-axis at angles slightly larger than $\varphi = \pi/2$. Thus, when moving along a circle of radius r_0, the direction of the SAM vector changes to the opposite upon reaching the point at angle $\varphi = \pi/2$. We note that at the circle point corresponding to $\varphi = \pi/2$, the SAM vector equals zero. The change of direction of the SAM vector lying in the focal plane upon passing a linear polarization point ($\mathbf{B} = 0$) may be termed the transverse spin Hall effect. It should be differentiated from the longitudinal spin Hall effect [8,9].

If the small axis of the polarization ellipse is zero, i.e., $\mathbf{B} = 0$, then the polarization ellipse reduces to a segment, i.e., polarization becomes linear. There is no polarization singularity at this point. When passing through such a point ($\mathbf{B} = 0$), the SAM vector, which is parallel to the focus plane in this case, changes its sign. Before the point with liner polarization ($\mathbf{B} = 0$), the SAM vector was directed nearly vertically downwards, i.e., the plane of the polarization ellipse is nearly perpendicular to the focus plane, and the polarization vector is rotating counterclockwise. On the contrary, after the point with linear polarization ($\mathbf{B} = 0$), the SAM is directed almost vertically upwards in the focus plane, the plane of the polarization ellipse is perpendicular to the focus plane, and the polarization vector is rotating clockwise. Both of these polarization ellipses form two "optical wheels", where the polarization ellipses are rotated like spokes in a wheel.

In (5), being $\cos(2\varphi)$-dependent, the longitudinal SAM projection changes sign four times on making a full circle. Hence, in the focal plane, there are four regions, in two of which the SAM projection is positive and in the other two negative. The separation of focal plane regions with different-sign longitudinal SAM components may be called the longitudinal spin Hall effect [8,9]. Summing up, in this section we demonstrated that given the initial light field (1), in the focal plane there are circles centered on the optical axis where the SAM vector lies in the focal plane and changes the direction to the opposite an even number of times. We have given this effect the name transverse spin Hall effect.

4. Polarization-Twisted Ribbons in the Focal Plane

Assuming initial field (1), let us now choose in the focal plane a different circle of radius r_1, on which the longitudinal projection B_z equals zero:

$$L(r_1) = I_{1,n-1} - I_{1,n+1} = 0. \tag{14}$$

In this case, the vector $\mathbf{B}$ lies in the focal plane, while the vector $\mathbf{A}$ 'almost' lies in the focal plane and is oriented along the horizontal axis, Equation (13). From (5), it is seen that at $0 < \varphi < \pi/4$ the longitudinal SAM projection is positive, $S_z = (1/2)(I_{2,n-2} - I_{2,n+2})(I_{2,n-2} + I_{2,n+2} + 2I_{0,n}\cos 2\varphi) > 0$ if $I_{2,n-2} - I_{2,n+2} > 0$ on the circle of radius r_1, whereas at $\varphi = \pi/2$ the longitudinal SAM projection is negative because $2I_{0,n} > I_{2,n-2} + I_{2,n+2}$. Hence, at some angle φ from the interval $\pi/4 < \varphi < \pi/2$, the longitudinal SAM projection becomes zero:

$$S_z = 0,\ I_{2,n-2} + I_{2,n+2} = 2I_{0,n}\cos 2\varphi. \tag{15}$$

In view of Equation (14), it follows from (5) that on the circle of radius r_1, the transverse SAM projections take a simpler form:

$$\begin{aligned} S_x &= 2M(r_1)\sin\varphi\cos 2\varphi, \\ S_y &= -2M(r_1)\cos\varphi\sin 2\varphi. \end{aligned} \tag{16}$$

The change of sign of the longitudinal SAM projection (1) means that at the focus, we observe a longitudinal spin Hall effect. When making a full circle of radius r_1, the longitudinal SAM component changes sign four times at any number n. We conclude that at small values of the angle φ, surfaces of the polarization ellipses centered on the circle of radius r_1 in the focal plane almost lie in the focal plane, "looking" along the optical axis. At an angle at which $S_z = 0$ (15), the polarization ellipse surfaces are perpendicular to the focal plane. At an angle somewhat larger than the angle in (15), the polarization ellipse surfaces get tilted oppositely, "looking" in the opposite direction to the optical axis. Hence, on a full circle centered on the optical axis lying in the focal plane, a surface constructed from the polarization ellipses "looks" twice along the optical axis (with the major axis directed almost along the x-axis), "looking" twice in the opposite direction to the optical axis (then, the ellipse major axis is directed oppositely to the x-axis). At "twis" points, which occur four times on the circle, defined by condition (15), the polarization plane "look" perpendicularly to the optical axis. Thus, we have shown that the longitudinal spin Hall effect is associated with the presence of two-sided polarization-twisted ribbons at the focus [4], unlike a one-sided polarization Mobius strip [1,2]. The number of twists of the twisted ribbon should coincide with the number of regions of alternating-sign longitudinal spin. Below, this conclusion is validated by the numerical simulation. We note that the number of areas with the spin of a different sign and the number of turns of the polarization ribbon is the same (in total, 4) and do not depend in this case on the topological charge of the linearly polarized optical vortex (1).

5. Other Types of Light Fields for Which Projections of Polarization Ellipses at the Focus Can Be Analytically Derived

5.1. Cylindrical Vector Fields

The Jones vector in the original plane of a cylindrical vector beam of n-th order (n is an integer) is given by:

$$\mathbf{E}(\varphi) = \begin{pmatrix} \cos n\varphi \\ \sin n\varphi \end{pmatrix}. \tag{17}$$

Relationships for the **E**-vector projections onto the focal plane from the original field in (17) have been known [8,12]:

$$\begin{aligned} E_x &= i^{n-1}(I_{0,n}\cos n\varphi + I_{2,n-2}\cos(n-2)\varphi), \\ E_y &= i^{n-1}(I_{0,n}\sin n\varphi - I_{2,n-2}\sin(n-2)\varphi), \\ E_z &= 2i^n I_{1,n-1}\cos(n-1)\varphi. \end{aligned} \tag{18}$$

In (18), the integrals $I_{\mu\nu}$ are defined by (3). Field projections in (18) can be expressed via projections of vectors **A** and **B** using Equation (8), then:

$$\begin{aligned} &\mathbf{E} = e^{i\gamma}(\mathbf{A} + i\mathbf{B}), \\ &A_x = I_{0,n}\cos n\varphi + I_{2,n-2}\cos(n-2)\varphi, \\ &A_y = I_{0,n}\sin n\varphi - I_{2,n-2}\sin(n-2)\varphi, \\ &A_z = 0, \\ &B_x = 0, \\ &B_y = 0, \\ &B_z = 2I_{1,n-1}\cos(n-1)\varphi, \\ &\gamma = (n-1)\tfrac{\pi}{2}. \end{aligned} \tag{19}$$

From (19), the vectors **A** and **B** lying in the polarization ellipse plane are seen to be mutually orthogonal: **AB** = 0. Considering that $I_{0,n} > I_{1,n-1}$, the **A** vector corresponds to the polarization ellipse major axis, with the **B** vector corresponding to the minor axis. Considering that the **B** vector has just a longitudinal projection, it is perpendicular to the focal plane. Meanwhile, with the **A** vector having just transverse projections, it lies in the focal plane. At the same time, the spin density vector **S** perpendicular to the two above-said vectors is described by the projections:

$$\begin{aligned} S_x &= 4I_{1,n-1}\cos((n-1)\varphi)[I_{0,n}\sin(n\varphi) - I_{2,n-2}\sin((n-2)\varphi)], \\ S_y &= -4I_{1,n-1}\cos((n-1)\varphi)[I_{0,n}\cos(n\varphi) + I_{2,n-2}\cos((n-2)\varphi)], \\ S_z &= 0. \end{aligned} \tag{20}$$

Hence, we can see that the situation that we observed for field (1) just on a circle of radius r_0, for field (17), occurs in the whole focal plane. What is more, the field at the focus is linearly polarized when $\cos(n-1)\varphi = 0$, i.e., at angles $\varphi_p = \pi(1/2+p)/(n-1)$, where

$p = 0, 1, 2, \ldots$ At angles somewhat smaller than φ_p, the projection of the vector **B** is positive if $I_{1,n-1} > 0$, whereas at angles somewhat larger than φ_p, the projection of the vector **B** is negative. At the same time, the **A** vector lying in the focal plane hardly changes. We can infer that the spin density vector **S**, which also lies in the focal plane, on passing the angles φ_p changes the direction to the opposite. Thus, in the focal plane of field (17), there is no longitudinal spin Hall effect, but there is a transverse spin Hall effect. In other words, on an axis-centered circle of arbitrary radius in the focal plane, there are $4(n-1)$ regions such that the transverse spin components have an alternating sign in the neighboring regions. Besides, lying on this circle are $4(n-1)$ points at which light is linearly polarized (the **B** vector equals zero) and the transverse spin also equals zero, $\mathbf{S}_\perp = 0$. So, when making a full axis-centered circle of any radius lying in the focal plane, the polarization ellipse always remains perpendicular to the focal plane, with the polarization vectors rotating in the ellipse plane like spokes of a wheel. Thus, field (17) produces at the tight focus a "photonic wheel" effect [15]. A remarkable finding is that while traversing the focal plane, the light wave is not transversely polarized, as the wave vector and polarization ellipse lie in the same plane. In summary, we found the following unique polarization properties of the cylindrical vector field (17) in the focus plane: (a) the longitudinal component of the SAM density vector is zero throughout the whole focus plane (i.e., the longitudinal spin Hall effect does not arise in the focus plane); (b) the SAM vector lies in the focus plane $\mathbf{S}_\perp$, and the major axis of the polarization ellipse **A** also lies in the focus plane; thus, the polarization ellipse itself is perpendicular to the focus plane and its minor axis **B** is also perpendicular to the focus plane (optical wheels); (c) the wave vectors of the light field (17) are perpendicular to the focus plane (laminar energy flow) and lie in the plane of the polarization ellipses (i.e., the polarization vector can coincide with the wave vector in a certain moment of time).

5.2. An Azimuthally Polarized Optical Vortex

Below, we analyze another example of an original vector light field that allows obtaining analytical relationships for projections of the major and minor axes of the polarization ellipse at the tight focus. An original azimuthally polarized optical vortex of topological charge n is described by the Jones vector:

$$\mathbf{E}(\varphi) = \exp(in\varphi)\begin{pmatrix} -\sin\varphi \\ \cos\varphi \end{pmatrix}. \tag{21}$$

A specific feature of light field (21) is that at its tight focus, the longitudinal projection of the **E**-vector equals zero. At the center of a linearly polarized light field (21), there is a V-point polarization singularity where the linear polarization vector is uncertain. For the V-point polarization singularity, the Poincare-Hopf index is $\eta = 1$, which means that when making a full circle about the beam center in the original plane, the linear polarization vectors make a full turn.

According to Richards-Wolf theory [12], all projections of the **E**-vector onto the focal plane take the form [16]:

$$\begin{aligned} E_x &= \frac{i^{n+1}}{2} e^{in\varphi}\left[e^{i\varphi}R(r) + e^{-i\varphi}T(r)\right], \\ E_y &= \frac{i^n}{2} e^{in\varphi}\left[e^{i\varphi}R(r) - e^{-i\varphi}T(r)\right], \\ E_z &= 0, \\ R(r) &= (I_{0,n+1} + I_{2,n+1}), \\ T(r) &= (I_{0,n-1} + I_{2,n-1}). \end{aligned} \tag{22}$$

The first two equations in (22) can be rearranged to Equation (7) by explicitly expressing projections of vectors of the major and minor axes of a polarization ellipse in the focal plane:

$$\begin{array}{l} \mathbf{E} = e^{i\gamma}(\mathbf{A} + i\mathbf{B}), \\ A_x = \frac{1}{2}[R(r)\cos(n+1)\varphi + T(r)\cos(n-1)\varphi], \\ A_y = \frac{1}{2}[R(r)\sin(n+1)\varphi - T(r)\sin(n-1)\varphi], \\ A_z = 0, \\ B_x = \frac{1}{2}[R(r)\sin(n+1)\varphi + T(r)\sin(n-1)\varphi], \\ B_y = \frac{1}{2}[-R(r)\cos(n+1)\varphi + T(r)\cos(n-1)\varphi], \\ B_z = 0, \\ \gamma = (n+1)\frac{\pi}{2}. \end{array} \quad (23)$$

Putting n = 1, (23) is rearranged to:

$$\begin{array}{l} A_{x,1} = \frac{1}{2}[R(r)\cos 2\varphi + T(r)], \\ A_{y,1} = \frac{1}{2}R(r)\sin 2\varphi, \\ A_z = 0, \\ B_{x,1} = \frac{1}{2}R(r)\sin 2\varphi, \\ B_y = \frac{1}{2}[-R(r)\cos 2\varphi + T], \\ B_z = 0. \end{array} \quad (24)$$

The dot product of the vectors **A** and **B** equals: **AB** = $RT\sin(2n\varphi)/2$, suggesting that these vectors form the polarization ellipse axes only at n = 0 (azimuthal polarization). At other values of n, although lying in the focal plane, the **A** and **B** vectors are mutually orthogonal only on circles of certain radius when either $R(r)$ = 0, or $T(r)$ = 0, or at angles $\varphi = \pi p/(2n)$, p = 0,1,2,... From (24) we find that a C-point of circular polarization at the tight focus center has the index Ic = 2, because upon making a circle around the optical axis, the polarization ellipse major axis makes four half-turns, as projections of the **A** vector in (24) depend on the double azimuthal angle.

At the tight focus, field (21) has just a longitudinal SAM vector projection:

$$S_z = 2\mathrm{Im}\left(E_x^* E_y\right) = 2\left(A_x B_y - A_y B_x\right) = \left(T^2(r) - R^2(r)\right)/2. \quad (25)$$

With the longitudinal SAM vector projection in (25) being φ-independent, it changes sign or equals zero on circles of certain radius. So, the intensity distribution at the focus has radial symmetry: $I(r) = |\mathbf{A}|^2 + |\mathbf{B}|^2 = \left(R^2(r) + T^2(r)\right)/2$. In the focal plane, on a circle of radius r_2 on which an equality $R(r_2) = T(r_2)$ holds, field (21) is linearly polarized because the longitudinal SAM component in (25) equals zero, S_z = 0. However, considering that the vectors **A** and **B** are mutually orthogonal and form polarization ellipse axes only at certain rays tilted at angles $\varphi = \pi p/(2n)$, p = 0, 1, 2, ..., when $\sin(2n\varphi)$ = 0, it is exactly under these conditions that the **B** vector equals zero and field (22) is linearly polarized. At $R(r)T(r)\cos(2n\varphi) = 0$, the vectors **A** and **B** have the same absolute value, which occurs on axis-centered circles with radii such that either $R(r)$ = 0 or $T(r)$ = 0, or at angles $\varphi = \pi/(4n)+\pi p/(2n)$, p = 0, 1, 2, ... and field (22) is circularly polarized (C-line polarization singularity). On the axis-centered circles in the focal plane for which $|T(r)| > |R(r)|$, the spin density S_z is positive and, vice versa, on circles where $|T(r)| < |R(r)|$, the spin density is negative. Thus, we have shown that at the tight focus of field (21), the sign of the longitudinal spin component S_z is alternating. Assuming a positive S_z on some radius in the focal plane, we find that with increasing radius, S_z is decreasing before becoming zero and then negative with further increasing radius. Such a behavior pattern of the longitudinal SAM component is a manifestation of a radial longitudinal spin Hall effect. It is of interest to analyze the behavior of the polarization ellipse surface in the focal plane ($A_z = B_z = 0$). As we are moving away from the optical axis along the radial variable, we find the polarization ellipse surface to be "looking" in the optical axis direction as far as $S_z > 0$. Meanwhile, at S_z = 0, the polarization ellipse shrinks to a segment (it is exactly where the ellipse surface experiences a twist). Finally, after traversing the $S_z = 0$ point, we find that $S_z < 0$, meaning that the polarization ellipse surface is "looking" in the opposite direction to the optical axis.

6. Numerical Modeling

In this section, based on Richards-Wolf formalism [12], we derive projections of the **E**-vector for some original light fields and intensity patterns at the tight focus. Next, using Berry formulae (7) for the same light fields, we calculate the coordinates of the major and minor axis vectors of the polarization ellipses centered in the focal plane. The wavelength is 532 nm, and the numerical aperture is NA = 0.95.

In Figure 1, depicted as a vertically elongated, inhomogeneous yellow-and-red ring, there is an intensity pattern at the tight focus for the original field (1) at $n = 3$. The white color marks the maximum intensity, yellow marks medium intensity, red marks low intensity and black marks zero intensity. In compliance with Equation (6), the on-axis intensity in Figure 1 is seen to be zero. Equation (6) also suggests that the intensity pattern should have two maxima on a near-circular ring located on the vertical or horizontal axis, depending on the sign of the expression in the round braces, which is multiplied by cos(2φ). The maximum intensity values (marked white) in Figure 1 are seen to be located on the vertical axis; hence, we infer that the expression in (6) that is multiplied by cos(2φ) is negative. Although the on-axis intensity is zero, the near-axis transverse amplitude of field (2) can effectively be expressed as

$$\begin{pmatrix} E_x \\ E_y \end{pmatrix} \approx -e^{i\varphi} I_{2,1} \begin{pmatrix} 1 \\ i \end{pmatrix}. \tag{26}$$

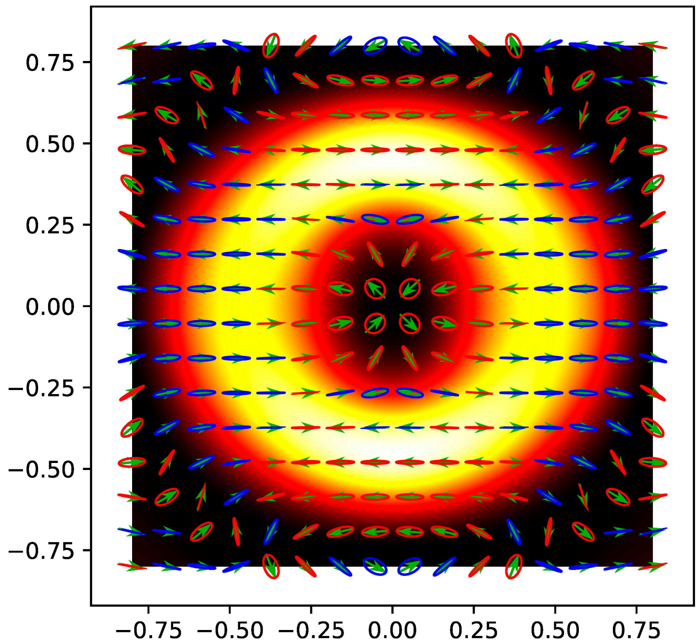

Figure 1. Intensity distribution (a slightly elliptical white-yellow-red ring) and projections of polarization ellipses onto the focal plane for the original field (1), describing a horizontally linearly polarized optical vortex ($n = 3$). In-ellipse arrows mark the direction of the major axis of the polarization ellipse. Blue ellipses correspond to the left-handed circular polarization and negative longitudinal SAM projection ($S_z < 0$), with red ellipses corresponding to right-handed circular polarization and positive longitudinal spin ($S_z > 0$).

Relationship (26) suggests that in the optical axis vicinity, the light is near right-handed circularly polarized. In Figure 1, inside the light-colored intensity ring, the polarization ellipses are near circular and marked red, indicating the right-handed circular polarization. From Figure 1, on a full circle around the optical axis, the major axis of the ellipses within the intensity ring is seen to rotate by 2π, implying that Ic = 1. The same conclusion can be drawn from Equation (26), as near the optical axis in the focal plane, the topological charge equals 1 (at n = 3).

In Figure 1, the yellow ellipse-shaped intensity pattern is seen to be fringed with inner and outer red ellipses. A closer look at the inner red intensity ellipse reveals that the polarization vectors are marked blue at the top and bottom and red on either side. So, we infer that the longitudinal SAM component, S_z, within the intensity ring is negative at the top and bottom and positive on either side. Therefore, there are four regions with opposite-sign spin, which is a manifestation of the longitudinal spin Hall effect. Vice versa, the outer red intensity ellipse is fringed with red arrows of polarization at the top and bottom and blue arrows on either side. So, in the outer red intensity ellipse, the longitudinal SAM component, S_z is positive at the top and bottom and negative on either side, also showing that there are four regions with the opposite-sign spin.

Moving along the edge of the yellow intensity ellipse, we find that at the boundary where the red arrows change to the oppositely directed blue ones, the major axis vector of the polarization ellipse experiences an abrupt flip-over in 3D space. When making a full circle around the optical axis, the major axis vector forms a 3D two-sided strip with an even umber of 'lip-overs', equal to the number of regions with the opposite-sign longitudinal spin. Such a strip with an even number of half-turns is called a polarization-twisted ribbon [6].

In addition, it is seen from Figure 1 that upon moving along the ellipse around its center, approximately half-way in the yellow intensity pattern, the direction of the major axis of polarization ellipse changes to the opposite six times at uniform 60-degree intervals. Thus, farther from the optical axis in the focal plane, the polarization singularity index of field (1) equals Ic = 3, being equal to the topological charge (n = 3) of the original field in (1).

Making note of the four blue arrows at the top of the internal red intensity ellipse in Figure 1, we can see that they twice change their direction to the opposite. Considering that the four blue-arrow polarization ellipses are narrow, we infer that the polarization ellipses are nearly perpendicular to the focal plane. Their blue color means that the minor axis of the polarization ellipse is opposite to the optical axis, whereas the SAM vector is near vertical and almost in the focal plane (being slightly negatively tilted relative to the optical axis). Hence, for two of the four blue arrows, the spin vector **S** is directed nearly vertically upwards, being directed downwards for the other two. Such a spatial separation of focal regions with the oppositely directed transverse spin **S** (upwards and downwards in Figure 1) may be called a transverse spin Hall effect. Such reasoning based on Figure 1 agrees well with the theoretical conclusions from Equation (13).

Figure 2 depicts an intensity pattern (squeezed white-yellow-red ring) in the focal plane from the original cylindrical second-order vector beam of Equation (17) at n = 2. From (18), the intensity at the focus is seen to depend on cos(2φ), leading to two intensity maxima on the horizontal axis (marked white in Figure 2). Note that at the center, instead of an intensity null, there is an intensity minimum proportional to the term $I_{2,0}$ in (18). From (18), it follows that there are two zero-intensity points on the vertical axis, because at φ = π/2 and φ = 3π/2, field (18) has the only non-zero projection: $E_x = i(I_{2,0} - I_{0,2})$, which becomes equal to zero at $I_{0,2} - I_{2,0} = 0$. At these points of field (18), there are V-point polarization singularities where polarization is uncertain. From Figure 2, it can be seen that when making a full circle around these two points, the linear polarization vector rotates by 2π, similar to azimuthal polarization. That is, the said two V-points have the indices +1 (upper) and –1 (lower). At n = 2, the initial field (17) has an on-axis V-point with the index 2, which spits at the focus into two V-points, with the sum of their indices being equal to zero. It would seem that the polarization singularity index should not conserve upon tight focusing. However, when making a circle of a larger radius, the seeming contradiction is eliminated. When making a full circle along the outside (red) intensity ellipse, the linear polarization vectors make two full turns (four semi-turns); because of this, the field index in Figure 2 equals 2, coinciding with the original field index.

From Figure 2, the polarization vectors are seen to lie in the longitudinal planes and perpendicularly to the focal plane (forming photonic wheels), meaning that only linear polarization vectors (the major axes of polarization ellipses) lie in the focal plane. In Figure 2, blue arrows are seen to prevail in the upper right and lower left quadrants, with red arrows dominating the upper left and lower right quadrants. Red arrows mark the right-handed circular polarization, with the spin vector **S** in the focal plane being directed predominantly downwards. Blue arrows mark the left-handed circular polarization, with the spin vector directed mainly upwards. Thus, in the focal spot plane, we observe alternating regions of upwards- and downwards-directed transverse spin vectors, which is a manifestation of the transverse spin Hall effect. When moving along the intensity ellipse contour in the focal plane, we find that the polarization arrows are partly directed with and partly against the motion direction. Meanwhile, for same-color arrows, this suggests that the spin vector **S** is alternatively directed inwards and outwards of the ellipse. If two same-direction arrows are of different colors, the spin vector **S** is directed inwards for one and outwards for the other (different-color) circle. Such a behavior pattern of the spin vector can be called a transverse (radial) spin Hall effect. When moving along an axis-centered circle, we encounter arrows perpendicular to the circle. If two given arrows are different colors, the spin vector **S** is tangentially directed along the motion in one of them, being directed oppositely in the other. For two same-color, oppositely directed arrows, their respective spin vectors are directed with and against the motion-handedness. This effect may be called a transverse (azimuthal) spin Hall effect.

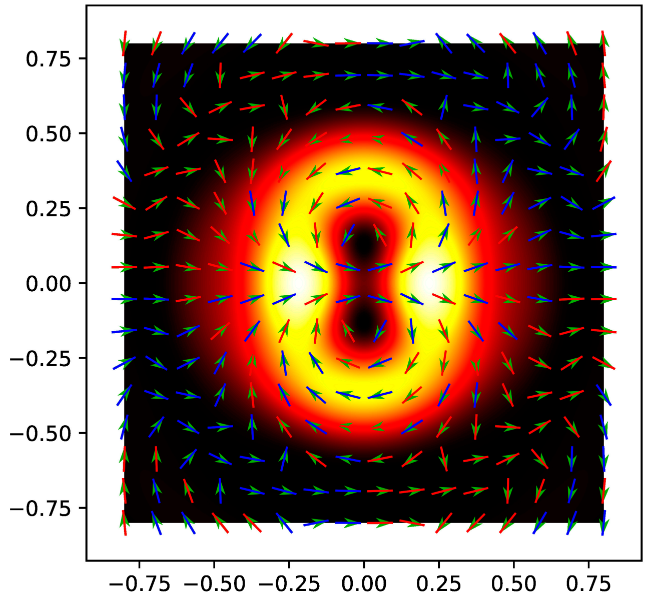

Figure 2. Intensity pattern (squeezed white-yellow-red ring) across the tight focus from the original cylindrical second-order vector beam in (17) at n = 2 and polarization ellipse projections onto the focal plane. In-ellipse arrows show the direction of the polarization ellipse major axis. Note that with the polarization ellipses being perpendicular to the focal plane, their projections on the plane coincide with the arrows. Blue arrows mark left-handed circular polarization, and red ones mark right-handed circular polarization. The axes are plotted in microns.

Figure 3 depicts intensity patterns across the focal spot generated by the initial field (21) at n = 1, with white-yellow areas marking the maximum intensity and violet-black areas showing the minimum intensity. In view of Equation (22) and putting n = 1, field (21) is seen to produce an on-axis C-point of right-handed circular polarization, with its polarization singularity index being equal to Ic = 2. Upon moving anticlockwise around the optical axis, the major axis vector of the polarization ellipse in Figure 3 makes four half-turns, or two full turns. When compared to the polarization singularity index for V-point in the original plane (η = 1), a larger singularity index value at the focus for the C-point (I_C = 2) is due to the fact that while in the original plane, the optical vortex topological charge (n = 1) has no effect on the singularity index of field (21), in the focal plane, the optical vortex changes the polarization pattern topology, increasing the polarization index value by 1 thanks to extra phase jumps by π.

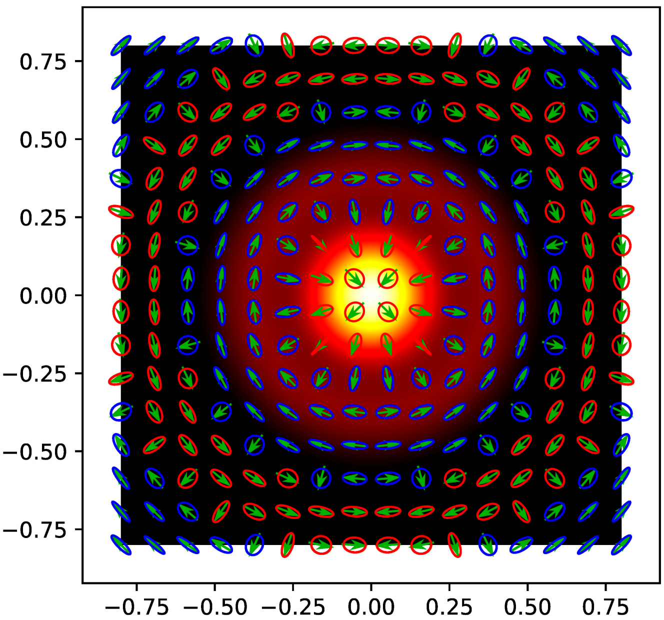

Figure 3. An intensity pattern (marked white-yellow-red) at the focus of an azimuthally polarized field in (21) at topological charge n = 1 and a pattern of polarization ellipse distribution in the focal plane. The green arrows inside the ellipses mark the major axis vector. Red ellipses mark right-handed elliptic polarization ($S_z > 0$), and blue ellipses mark left-handed elliptic polarization ($S_z < 0$). The axes are plotted in microns.

Moving away from the optical axis along an arbitrary radius, the major axis vector of the polarization ellipse in Figure 3 will form a non-closed strip in 3D space with half-turns found at distances of linear polarization.

7. Conclusions

The following optical polarization effects have been theoretically and numerically shown to occur at the tight focus of a linearly polarized optical vortex with topological charge n. When moving along a full circle around the optical axis in the focal plane, the major axis vectors of the polarization ellipse have been shown to make $2n$ half-turns. That is, in a vector field composed of the major axis vectors of the focal-plane-centered polarization ellipses, the polarization singularity index equals the topological charge of the original optical vortex. Irrespective of the topological charge, four regions have been found to occur in the focal plane in which the longitudinal SAM projection has an alternating sign, demonstrating a longitudinal Hall effect. We have shown that on moving along a closed, axis-centered (circular or elliptic) contour, the major axis vector of the polarization ellipse generates, in a 3D space, a two-sided twisted ribbon with an even number of half-turns, by analogy with a twisted ribbon in Ref. [6]. In the focal plane, regions have been found to occur in which the transverse spin vector projections located in the focal plane have an alternating handedness relative to the circular motion handedness. This is a manifestation of an azimuthal transverse spin Hall effect. We have also demonstrated that upon moving on a circle, the transverse spin vector projections on the circle radii can be alternatively directed either from or to the center, which is a manifestation of a radial transverse spin Hall effect.

The results obtained in this work can be employed for nanostructuring polarization-sensitive materials [17–21], for magnetization and data recording based on the inverse Faraday effect [22–25], for manipulating microparticles [26–28] as well as in optical microscopy [29–31].

Author Contributions: Conceptualization, V.V.K.; methodology, V.V.K., A.A.K. and Z.G.; software, A.A.K., A.K. and K.G.; validation, V.V.K.; formal analysis, V.V.K.; investigation, V.V.K. and A.A.K.; resources, V.V.K.; data curation, V.V.K.; writing—original draft preparation, V.V.K. and E.S.K.; writing—review and editing, V.V.K.; visualization, A.A.K., A.M.T. and S.S.S.; supervision, V.V.K.; project administration, V.V.K.; funding acquisition, V.V.K. and A.A.K. All authors have read and agreed to the published version of the manuscript.

Funding: The work was partly funded by the Russian Science Foundation under grant # 22-12-00137 (Theoretical background) and from the government project of the NRC "Kurchatov Institute" (numerical modeling).

Institutional Review Board Statement: Not applicable.

Informed Consent Statement: Not applicable.

Data Availability Statement: Data are contained within the article.

Conflicts of Interest: The authors declare no conflicts of interest. The funders had no role in the design of the study; in the collection, analyses, or interpretation of data; in the writing of the manuscript; or in the decision to publish the results.

References

1. Bauer, T.; Banzer, P.; Karimi, E.; Orlov, S.; Rubano, A.; Marrucci, L.; Santamato, E.; Boyd, R.W.; Leuchs, G. Observation of optical polarization Möbius strips. *Science* **2015**, *347*, 964–966. [CrossRef]
2. Wan, C.; Zhan, Q. Generation of exotic optical polarization Möbius strips. *Opt. Express* **2019**, *27*, 11516–11524. [CrossRef] [PubMed]
3. Freund, I. Multitwist optical Möbius strips. *Opt. Lett.* **2010**, *35*, 148–150. [CrossRef] [PubMed]
4. Freund, I. Optical Möbius strips, twisted ribbons, and the index theorem. *Opt. Lett.* **2011**, *36*, 4506–4508. [CrossRef]
5. Freund, I. Cones, spirals, and Möbius strips, in elliptically polarized light. *Opt. Commun.* **2005**, *249*, 7–22. [CrossRef]
6. Freund, I. Optical Möbius strips and twisted ribbon cloaks. *Opt. Lett.* **2014**, *39*, 727–730. [CrossRef] [PubMed]
7. Galvez, E.J.; Dutta, I.; Beach, K.; Zeosky, J.J.; Jones, J.A.; Khajavi, B. Multitwist Möbius strips and twisted ribbons in the polarization of paraxial light beams. *Sci. Rep.* **2017**, *7*, 13653. [CrossRef]
8. Kovalev, A.A.; Kotlyar, V.V. Spin Hall effect of double-index cylindrical vector beams in a tight focus. *Micromachines* **2023**, *14*, 494. [CrossRef]
9. Kotlyar, V.V.; Kovalev, A.A.; Kozlova, E.S.; Telegin, A.M. Hall effect at the focus of an optical vortex with linear polarization. *Micromachines* **2023**, *14*, 788. [CrossRef]
10. Kotlyar, V.V.; Kovalev, A.A.; Telegin, A.M. Generalized Poincaré Beams in Tight Focus. *Photonics* **2023**, *10*, 218. [CrossRef]
11. Berry, M.V. Index formulae for singular lines of polarization. *J. Opt. A: Pure Appl. Opt.* **2004**, *6*, 675–678. [CrossRef]
12. Richards, B.; Wolf, E. Electromagnetic diffraction in optical systems, II. Structure of the image field in an aplanatic system. *Proc. R. Soc. Lond. A* **1959**, *253*, 358–379. [CrossRef]
13. Kotlyar, V.V.; Nalimov, A.G.; Stafeev, S.S. Exploiting the circular polarization of light to obtain a spiral energy flow at the subwavelength focus. *J. Opt. Soc. Am. B* **2019**, *36*, 2850–2855. [CrossRef]
14. Barnett, S.M.; Allen, L. Orbital angular momentum and nonparaxial light beams. *Opt. Commun.* **1994**, *110*, 670–678. [CrossRef]
15. Aiello, A.; Banzer, P.; Neugebauer, M.; Leuchs, G. From transverse angular momentum to photonic wheels. *Nat. Photonics* **2015**, *9*, 789–795. [CrossRef]
16. Kotlyar, V.V.; Stafeev, S.S.; Kovalev, A.A. Reverse and toroidal flux of light fields with both phase and polarization higher-order singularities in the sharp focus area. *Opt. Express* **2019**, *27*, 16689–16702. [CrossRef] [PubMed]
17. Lei, Y.; Wang, H.; Shayeganrad, G.; Kazansky, P.G. Ultrafast laser nanostructuring in transparent materials for beam shaping and data storage [Invited]. *Opt. Mater. Express* **2022**, *12*, 3327–3355. [CrossRef]
18. Lu, X.; Wang, X.; Wang, S.; Ding, T. Polarization-directed growth of spiral nanostructures by laser direct writing with vector beams. *Nat. Commun.* **2023**, *14*, 1422. [CrossRef] [PubMed]
19. Wang, B.; Che, Y.; Zhong, X.; Yan, W.; Zhang, T.; Chen, K.; Xu, Y.; Xu, X.; Li, X. Cylindrical vector beam revealing multipolar nonlinear scattering for superlocalization of silicon nanostructures. *Photonics Res.* **2021**, *9*, 950–957. [CrossRef]
20. Bautista, G.; Kauranen, M. Vector-Field Nonlinear Microscopy of Nanostructures. *ACS Photonics* **2016**, *3*, 1351–1370. [CrossRef]
21. Pallarés-Aldeiturriaga, D.; Abou Khalil, A.; Colombier, J.P.; Stoian, R.; Sedao, X. Ultrafast Cylindrical Vector Beams for Improved Energy Feedthrough and Low Roughness Surface Ablation of Metals. *Materials* **2022**, *16*, 176. [CrossRef]

22. Yang, X.; Mou, Y.; Zapata, R.; Reynier, B.; Gallas, B.; Mivelle, M. An inverse Faraday effect generated by linearly polarized light through a plasmonic nano-antenna. *Nanophotonics* **2023**, *12*, 687–694. [CrossRef]
23. Wang, S.; Li, X.; Zhou, J.; Gu, M. All-optically configuring the inverse Faraday effect for nanoscale perpendicular magnetic recording. *Opt. Express* **2015**, *23*, 13530–13536. [CrossRef] [PubMed]
24. González-Alcalde, A.K.; Shi, X.; Ortiz, V.H.; Feng, J.; Wilson, R.B.; Vuong, L.T. Enhanced inverse Faraday effect and time-dependent thermo-transmission in gold nanodisks. *Nanophotonics* **2024**. [CrossRef]
25. Karakhanyan, V.; Eustache, C.; Lefier, Y.; Grosjean, T. Inverse Faraday effect from the orbital angular momentum of light. *Phys. Rev. B* **2022**, *105*, 045406. [CrossRef]
26. Zhao, Y.; Zhou, L.; Jiang, X.; Zhu, L.; Shi, Q. Optical Force Effects of Rayleigh Particles by Cylindrical Vector Beams. *Nanomaterials* **2024**, *14*, 691. [CrossRef]
27. Chen, Q.; Liu, P.; Fu, Y.; Zhang, S.; Zhang, Y.; Yuan, X.; Min, C. Monolayer Chiral Metasurface for Generation of Arbitrary Cylindrical Vector Beams. *Photonics* **2024**, *11*, 57. [CrossRef]
28. Yang, Y.; Ren, Y.; Chen, M.; Arita, Y.; Rosales-Guzmán, C. Optical trapping with structured light: A review. *Adv. Photonics* **2021**, *3*, 034001. [CrossRef]
29. Min, L.; Yunze, L.; Fang, L.; Ma, X.; Liu, Y.; Zheng, L.; Gao, J. Super-resolution optical microscopy using cylindrical vector beams. *Nanophotonics* **2022**, *11*, 3395–3420. [CrossRef]
30. Bautista, G.; Kakko, J.; Dhaka, V.; Zang, X.; Karvonen, L.; Jiang, H.; Kauppinen, E.; Lipsanen, H.; Kauranen, M. Nonlinear microscopy using cylindrical vector beams: Applications to three-dimensional imaging of nanostructures. *Opt. Express* **2017**, *25*, 12463–12468. [CrossRef]
31. Chen, R.; Agarwal, K.; Sheppard, C.J.; Chen, X. Imaging using cylindrical vector beams in a high-numerical-aperture microscopy system. *Opt. Lett.* **2013**, *38*, 3111. [CrossRef] [PubMed]